THE JOURNAL OF PHYSICAL CHEMISTRY A

Article

pubs.acs.org/JPCA

Nanostructured Diamine–Fullerene Derivatives: Computational Density Functional Theory Study and Experimental Evidence for their Formation via Gas-Phase Functionalization

Flavio F. Contreras-Torres,*[,†] Elena V. Basiuk,[†,§] Vladimir A. Basiuk,[‡,§] Víctor Meza-Laguna,[†] and Taras Yu. Gromovoy[∥]

[†]Centro de Ciencias Aplicadas y Desarrollo Tecnológico, Universidad Nacional Autónoma de México (UNAM), Circuito Exterior, Ciudad Universitaria 04510, México D.F., Mexico

[‡]Instituto de Ciencias Nucleares, UNAM, Circuito Exterior, Ciudad Universitaria 04510, México D.F., Mexico

[§]Dipartimento di Chimica IFM, Università degli Studi di Torino, Via P. Giuria 7, 10125 Torino, Italy

[∥]A. A. Chuiko Institute of Surface Chemistry, National Academy of Sciences of Ukraine, 17 Generala Naumova Street, 03164 Kiev, Ukraine

ABSTRACT: Nanostructure derivatives of fullerene C_{60} are used in emerging applications of composite matrices, including protective and decorative coating, superadsorbent material, thin films, and lightweight high-strength fiber-reinforced materials, etc. In this study, quantum chemical calculations and experimental studies were performed to analyze the derivatives of diamine–fullerene prepared by the gas-phase solvent-free functionalization technique. In particular, the aliphatic 1,8-diamino-octane and the aromatic 1,5-diamino-naphthalene, which are diamines volatile in vacuum, were studied. We addressed two alternative mechanisms of the amination reaction via polyaddition and cross-linking of C_{60} with diamines, using the pure GGA BLYP, PW91, and PBE functionals; further validation calculations were performed using the semiempirical dispersion GGA B97-D functional which contains parameters that have been specially adjusted by a more realistic view on dispersion contributions. In addition, we looked for experimental evidence for the covalent functionalization by using laser desorption/ionization time-of-flight mass spectrometry, thermogravimetric analysis, and atomic force microscopy.

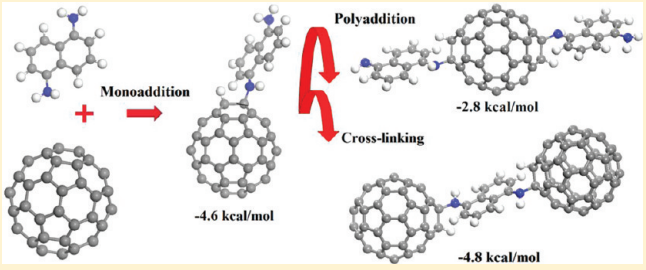

1. INTRODUCTION

Pristine fullerene C_{60} is an *n*-type semiconductor with the highest mobility of 0.08 $cm^2/(V{\cdot}s)$.[1] In conjunction with its intrinsic zero-dimensionality, such electronic property stimulated the preparation of fullerene C_{60} thin films and their versatile studies under variable physical conditions.[2−5] Moreover, high electron mobility can furthermore be enhanced by using organic charge transporting materials,[6−8] and thus extensive research is under way to improve new promising electronic fullerene-based devices.[9−11] In this context, small planar conjugated systems containing two $-NH_2$ groups, such as phenyl and naphthalene amine-derivatives (e.g., 1,5-diaminonaphthalene, 1,8-diaminonaphthalene, *o*-phenylenediamine, etc.),[12−14] can also be expected to form conducting materials by functionalization with inorganic materials. For instance, 1,5-diaminonaphthalene has been intercalated onto the saponite matrix to form organic–inorganic composites which show electronic bands with a gap of ca. 1 eV suggesting semiconducting behavior.[15] The complex chemistry of product mixtures synthesized by the reaction between amines and fullerene C_{60} was reviewed elsewhere.[16] A number of possible technical applications of these products have recently been reported, such as the immobilization of amino-fullerenes onto silica support for accelerating the photochemical $^1O_2$ production and increasing the efficiency of pollutants degradation and viral inactivation.[17]

Theoretical studies of amine–fullerene derivatives have been carried out mainly by means of density functional methods.[18−20] A systematic analysis of possible nucleophilic polyaddition of methylamine was recently reported,[18,19] and the results confirmed that the monoaddition onto C_{60} preferentially takes place onto the 6,6 junction of pyracylene unit. At the PW91/DN level of theory, the monoaddition of methylamine onto the 6,6 junction of the pyracylene unit in C_{60} is ca. 400% energetically more favorable as compared to the addition onto the 5,6 junction. By increasing the basis set with polarization functions on all atoms, the DNP basis set produced a variation of 0.4 kcal mol^{-1}, which is only 2.3% of its energy of formation. In comparison, at the B3LYP/STO-3G level of theory, the difference between the calculated values for the 5,6 adduct and 6,6 adduct in C_{60} + nonylamine adducts was ca. 21 kcal mol^{-1}, or 92% energetically more stable for the 6,6

Received: December 1, 2011
Revised: January 16, 2012
Published: January 25, 2012

adduct.[9] Because of the fact that the reaction stoichiometry varies depending on the size of the amine reactant molecule, the theoretical analysis of the polyaddition products of C_{60}+methylamine indicates that the penta adduct is the most exothermic product ($\Delta E = -10.2$ kcal mol^{-1}) and then starts to increase at $n \geq 6$, apparently due to growing steric hindrance.[18] Although a mixture of isomers is produced for each stoichiometry, and the composition of the mixture only can be defined by the Boltzmann distribution of the relative free energies of the isomers at the temperature of formation, a very small energy difference of less than 1.4 kcal mol^{-1} was found with respect to the calculated energy of formation for the biadduct product. The latter may indicate that the unreacted second amino groups of diamine molecules can also become anchors for cross-linking a second fullerene molecule; however, this mechanism will also depend on the size and structure of diamines, as, for example, was reported for cross-linked amine-modified silica aerogel with epoxides.[21] While for smaller amine molecules (e.g., 2-methylaziridine) the average amine/fullerene C_{60} ratio can be as large as 10:1,[22] for long-chain aliphatic amines it decreases substantially. The lowest average number of amine reactant added, ≥1, was reported for dodecylamine;[23] for the gas-phase reaction of silica-supported fullerene with nonylamine the number of nonylamine molecules attached to fullerene was reported to be less than three.[9]

The explanation of reaction mechanisms has a paramount importance for the synthesis of functionalized carbon nanomaterials, which experimentally is carried out by the gas-phase solvent-free technique.[9,11,24−29] Local parameters such as pyramidalization angles[18,30] or Fukui indices[31] of the functionalized carbon atoms of fullerene have previously been employed to analyze and compared the most favorable amine−fullerene derivatives. Nevertheless, none of the theoretical studies mentioned above considered the C−N bond formation through the analysis of the entire chemical process by looking for reaction complex, transition states, and possible products. In an attempt to fill this gap, in the present study we focus on the mechanism of formation of amine−fullerene derivatives considering the plausible formation of cross-linked products as well as the formation of stacking polyfunctional C_{60} + amine complexes. Such polyadducts can experimentally be detected using mass spectrometric techniques, as previously demonstrated in the adducts with up to six nonylamine moieties attached to fullerene.[9] Because of the fact that the complex mixtures of products generated upon reacting fullerene C_{60} with diamines are highly problematic to characterize experimentally, in this study we appealed to theoretical methods to explore the mechanisms of addition of methylamine (MA), ethylenediamine (ED), 1,8-diamino-octane (DAO), and 1,5-diamino-naphthalene (DAN) onto fullerene C_{60}. These diamine molecules have been chosen since they have already been employed in our previous experimental studies.[11,25,32] Looking for experimental evidence for the cross-linking mechanism with diamines, both DAO and DAN-functionalized fullerene C_{60} derivatives were analyzed by laser desorption/ionization time-of-flight mass spectrometry (LDI-TOF MS), thermogravimetric analysis (TGA), and atomic force microscopy (AFM).

2. THEORETICAL BACKGROUND

Density functional theory (DFT)[33] proposes to solve electronic structure problems using as a fundamental variable the electron charge density, $\rho(\vec{r})$; formally it is based on the Hohenberg and Kohn theorems[34] and computationally is applied using the Kohn−Sham method (KS) through of a mean-field approach.[35] The KS method represents the density as a linear combination of the inner products of spin−orbital functions $\rho(\vec{r}) = \sum_i |\phi_i^{KS}(\vec{r})|^2$ and the energy as a functional of $\rho(\vec{r})$ as

$$E^{KS-DFT}[\rho] = T_s[\rho] + J[\rho] + E_{XC}[\rho] + \int d\vec{r}\rho(\vec{r})\upsilon_{ext}(\vec{r}) + V_{NN} \quad (1)$$

The contribution of $E_{XC}[\rho]$ is the exchange-correlation energy, which includes the electron exchange interaction as well as the many-body contribution to the kinetic, $T_s[\rho]$, and electron−electron repulsion, $J[\rho]$, potentials; however, the explicit expression of $E_{XC}[\rho]$ remains unknown. The $\upsilon_{ext}(\vec{r})$ term is the external potential generated by the nuclei and felt by electrons, and V_{NN} is the nuclear repulsion energy for a fixed nuclear configuration. There are many approaches that have shown satisfactory results; such approaches have been grouped into *generations* that remember the Jacob ladder's rungs.[36] The most used are based on the local spin density approximation (LSDA) or generalized gradient approximation (GGA);[37] however, the major source of error in LSDA is the exchange energy, $E_X[\rho]$.[38] The conventional density-gradient expansion does not provide satisfactory correction to the local-density approximation,[33] and the general drawback of all common pure GGA functionals, including hybrids such as the most popular B3LYP (which replace part of the local exchange by nonlocal Hartree−Fock exchange), is that they cannot describe long-range electron correlations that are responsible for the dispersive energies (i.e., London forces).[39,40] Neglect of dispersion can result in wrong binding energies and wrong geometries; the origins of these difficulties are mainly attributed to the incorrect cancellation of electron self-interaction.[41] To avoid this problem several strategies including adiabatic connection formalism[42,43] and semiempirical dispersion corrections,[40,44] among others,[45−49] have been developed.

From observations, it is well-known that the dispersion energy contributes asymptotically to the potential energy in long-range interactions as $U_{disp} \approx -R^{-6}$.[50] It has been proposed[51] to simply add an empirical term to account for the missing dispersion energies, that is, $E_{DFT-D} = E^{KS-DFT} + E^{disp}$, where E^{KS-DFT} is the usual self-consistent Kohn−Sham energy as obtained from eq 1. The empirical dispersion correction, E^{disp}, is based on an atom pairwise treatment[51−55]

$$E^{disp} = -s_6 \sum_{N-1}^{i=1} \sum_{N}^{j=i+1} f(R_{ij}) \frac{C_6^{ij}}{R_{ij}^6} \quad (2)$$

Here, N is the number of atoms in the system, C_6^{ij}, denotes the dispersion coefficient for atom pair ij that can be determinate by a geometric mean, $C_6^{ij} = (C_6^i C_6^j)^{1/2}$, and R_{ij} is an interatomic distance. The scaling parameter $s_6 = |\nabla\rho(\vec{r})|/\rho^{4/3}$ is set to different values as a function of the adopted functional; to avoid near singularities for small R, a damping function $f(R_{ij}) = \{1 + \exp[-\alpha(R_{ij}/R_{ij}^0 - 1)]\}^{-1}$ models a Fermi−Dirac-type distribution.

In this work, we used the $E_{XC}[\rho]$ proposed by Grimme[54] known as B97-D. This functional is based on Becke's GGA functional introduced in 1997[56] and is likely the most accurate semiempirical GGA available with the broadest range of applicability (e.g., helical conformational long-chain peptides,[51] supramolecular chemistry,[44,52,54] noncovalent complexes,[55]

Table 1. Energies[a] (in kcal mol^{-1}) Relative to the Level of Isolated Reactants as Calculated with the Pure GGA-DFT BLYP, PW91, and PBE Functionals (in Conjunction with the DNP Basis Set) for the Reaction Complexes (RC), Transition States (TS), and Products (P) in the Addition Reaction of Methylamine (C_{60} + MA), Ethylenediamine (C_{60} + ED), 1,8-Diamino-Octane (C_{60} + DAO), and 1,5-Diaminonaphthalene (C_{60} + DAN) with Fullerene C_{60}

	BLYP			PW91			PBE		
system	ΔE_{RC}	ΔE_{TS}	ΔE_{P}	ΔE_{RC}	ΔE_{TS}	ΔE_{P}	ΔE_{RC}	ΔE_{TS}	ΔE_{P}
C_{60} + MA	−1.8	75.4	4.6	−2.6	70.1	−3.2	−2.2	71.4	−2.6
C_{60} + ED	−2.2	71.8	4.6	−3.3	52.8	−3.4	−2.8	53.4	−2.9
C_{60} + DAO	−0.1	42.7	8.1	−0.8	32.2	0.5	0.5	32.7	1.0
C_{60} + DAN	0.2	53.7	12.2	−1.4	43.1	4.2	1.1	43.9	4.9

[a]Energies relative to the isolated fullerene C_{60} and amine molecules; for example, $\Delta E_{C_{60}+MA} = (\Delta E_{C60} - \Delta E_{MA})$.

Table 2. Energies of Formation[a] (in kcal mol^{-1}) as Calculated with the Pure GGA BLYP, PW91, and PBE Functionals (in Conjunction with the DNP Basis Set) and the Semiempirical Dispersion GGA B97-D Functional (in Conjunction with the 6-31G(d,p) Basis Set) for the Amine Diaddition Products C_{60} + $(DAO)_2$ and C_{60} + $(DAN)_2$ as Well as for the Cross-Linked $(C_{60})_2$ + DAO and $(C_{60})_2$ + DAN Products[b]

	pure GGA-DFT						semiempirical dispersion GGA-DFT-D			
system	BLYP	$\Delta\Delta E$	PW91	$\Delta\Delta E$	PBE	$\Delta\Delta E$	B97-D	$\Delta\Delta E$	B97-D (ZPE)	$\Delta\Delta E$
C_{60} + DAO	8.1		0.5		1.0		−7.3		−5.5	
$(C_{60})_2$ + DAO	5.4	−2.7	−2.8	−3.3	−2.4	−3.4	−7.3	−0.1	−5.5	0.0
C_{60} + $(DAO)_2$	6.9	−1.2	−1.1	−1.6	−0.6	−1.6	−5.6	1.7	−4.0	1.5
C_{60} + DAN	12.2		4.2		4.9		−4.6		−3.1	
$(C_{60})_2$ + DAN	12.1	−0.1	3.8	−0.4	4.3	−0.6	−4.8	−0.2	−3.3	−0.1
C_{60} + $(DAN)_2$	13.7	1.5	5.2	1.0	5.8	0.9	−2.8	1.8	−1.6	1.6

[a]Energies of formation relative to C_{60}+diamine compounds; for example, $\Delta\Delta E_{(C60)2+DAO} = (\Delta E_{(C60)2+DAO} - \Delta E_{C60+DAO})$. [b]Zero-point energy corrected values are also specified as B97-D (ZPE).

etc.) where both electrostatic and dispersive interactions are of paramount importance.

3. COMPUTATIONAL METHODS AND EXPERIMENTAL DETAILS

3.1. Computational Methods. Full all-electron treatment structure calculations were performed using the DMol3 numerical-based density-functional computer software implemented in the Material Studio Modeling 3.1 package from Accelrys, Inc.[57] Initially, the pure GGA BLYP,[58,59] PW91,[60] and PBE[61] functionals were tested. We chose BLYP and PW91 since both belong to the most frequently used density functionals and because their exchange parts represent the two extreme behavior at large density gradients. While Becke exchange functional[58] used in BLYP is the most strongly divergent exchange functional, PW91 is the only exchange functional that converges as the enhancement factor $F = F(s)$ approaches asymptotically to 0 for $s \rightarrow \infty$ (in the LSDA approximation, $F(s) = 1$). PW91 and PBE are generally regarded as essentially equivalent; that is, they produce similar numerical results for many properties including atomization energies. PW91 has previously been employed in similar works,[18,19] and thus in the present study, it also was tested for comparison. PBE is a functional used more seldom; it takes into account the exchange functional part similarly to the Becke's formula and at least qualitatively accounts for some dispersive interactions.[52]

Double-numerical plus polarization basis set (DNP) was employed to describe the electron density. The DNP basis set corresponds to a double-ζ quality basis set with a p-type polarization function added on hydrogen atoms, and d-type polarization functions added on carbon and nitrogen atoms; it is comparable to 6-31G(d,p) Gaussian basis set, providing a better accuracy at a similar basis set size.[62] Moreover, Delley[63] has shown that the use of numerical atomic orbitals implemented in the DMol3 package generates very small basis set superposition error (BSSE) because of nearly perfect atomic orbitals for the separated atom limit. Convergence tolerance and orbital cutoff quality were selected with fine criteria, and a global orbital cutoff of 3.7 Å was employed on the basis set definitions. We have tested these theoretical levels to study bimolecular interactions in carbon nanomaterials[31,64−66] and found it to be very convenient in the studies on related carbon nanocluster models; however, it is the first time we study the entire process of chemical reactions using these methodology. All the pure GGA-DFT energies are specified in Table 1 for describing the entire process of the monoaddition reaction and in Table 2 for describing the polyaddition and cross-linking mechanisms.

Further validation calculations were performed using semiempirical GGA-DFT methods, in particular those that contain parameters that have been specially adjusted by a more realistic view on dispersion contributions, DFT-D. The semiempirical GGA B97-D functional,[52] in conjunction with the 6-31G(d,p)[67] basis set as implemented in the Gaussian09 (revision A.02) package,[68] was employed to study the formation of the complexes C_{60} + DAO and C_{60} + DAN. The results for the interaction energies, ΔE, and zero-point corrected energies B97-D(ZPE) are shown in Table 2 for comparison with the electronic GGA-DFT energies.

A comparative analysis of the relative stability of the complexes with respect to their KS-DFT energies was performed using the variational supramolecular approach

$$\Delta E_R = E_R - (E_A + E_{C60})$$

dx.doi.org/10.1021/jp211577k | J. Phys. Chem. A 2012, 116, 1663−1676

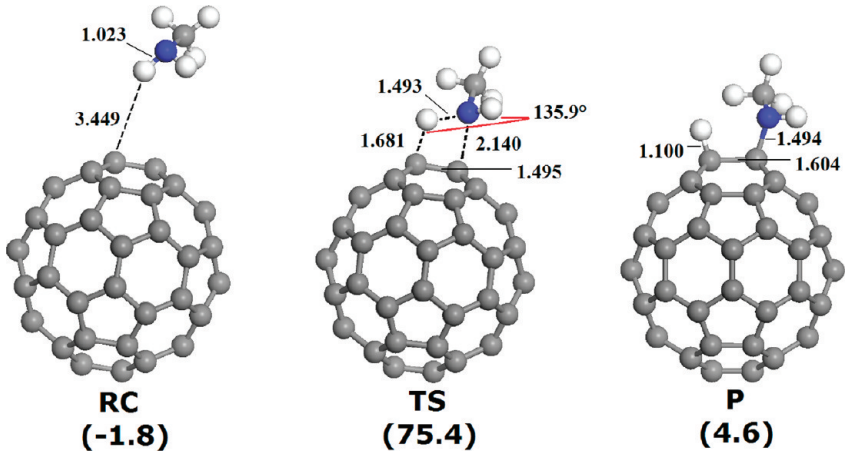

Figure 1. Optimized geometries for RC, TS and P for the functionalization of fullerene C_{60} with methylamine, as computed at the BLYP/DNP level of theory. Selected interatomic distances (in Ångstroms), angles (in degrees), and energies (in kcal mol^{-1}; relative to the level of isolated reactant species) are specified.

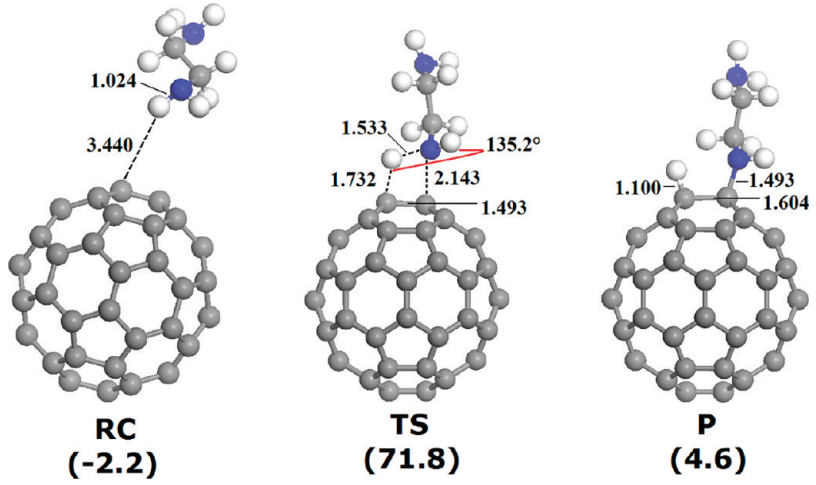

Figure 2. Optimized geometries for RC, TS, and P for the functionalization of fullerene C_{60} with ethylenediamine, as computed at the BLYP/DNP level of theory. Selected interatomic distances (in Ångstroms), angles (in degrees), and energies (in kcal mol^{-1}; relative to the level of isolated reactant species) are specified.

where E is the absolute KS-DFT energy; R denotes reaction complex (RC), transition state (TS) or product (P); A is the corresponding isolated amine molecule (MA, ED, DAO, or DAN), and C_{60} is isolated fullerene component. All stationary point geometries were fully optimized and characterized as minima (no imaginary frequencies) or first-order saddle points (one imaginary frequency) by calculations of vibrational frequencies. The first-order saddle points (i.e., transitions states, TS) were found by using the linear synchronous transit (LST)[64] technique. LST performs a single maximization, bracketing the maximum between the reactants and products. Furthermore, in all cases when transition states were found by LST maximum technique, they were reoptimized by a full conjugate gradient minimization (LSTCG) calculation, from the nondistorted LST optimization geometry. LSTCG is a method of interpolating geometrically between reaction complexes and products to generate a reaction pathway, and thus these calculations require a trajectory rather than a single model.[70]

3.2. Experimental Details. DAO and DAN, both from Alfa Aesar (98 and 97% purity, respectively) were placed each along with 50 mg of pristine fullerene C_{60} powder from MER Corp. (99.5% purity) inside Pyrex ampules at the 1:2 w/w (diamine/fullerene) ratio and then were pumped out to ca. 10^{-2}–10^{-1} Torr and sealed. The compounds were previously dehumidified in a vacuum for 1 h at room temperature (for diamines) and at 120 °C (for fullerene C_{60}). The reactants mixed and sealed into ampules were placed to a cylindrical furnace to carry out the solvent-free amination. The gas-phase functionalization with DAO and DAN, which are volatile at temperatures above 150 °C in vacuum, was performed as reported elsewhere.[11,25,71,72] More precisely, the reaction temperatures were 170 °C in the case of DAO and 220 °C in the case of DAN. After completing the reaction and cooling down, the ampules were opened and heated again at 150 °C (DAO) and 180 °C (DAN) under vacuum for 2 h to eliminate the excess of diamine.

For the laser desorption/ionization time-of-flight (LDI-TOF) mass spectrometry, the samples dispersed in methanol were deposited onto a standard steel target and dried under ambient conditions. The measurements were performed using an Autoflex II LRF 20 Bruker Daltonics instrument, equipped with a pulsed nitrogen laser of λ = 337 nm with a pulse width of

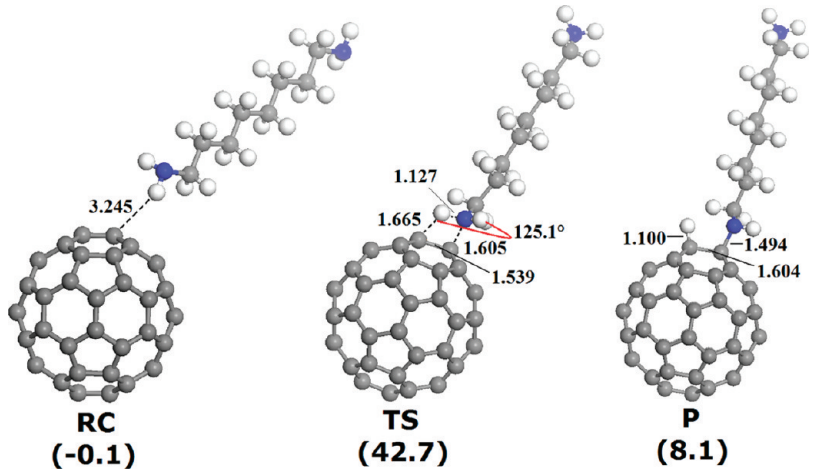

Figure 3. Optimized geometries for RC, TS, and P for the functionalization of fullerene C_{60} with DAO, as computed at the BLYP/DNP level of theory. Selected interatomic distances (in Ångstroms), angles (in degrees), and energies (in kcal mol^{-1}; relative to the level of isolated reactant species) are specified.

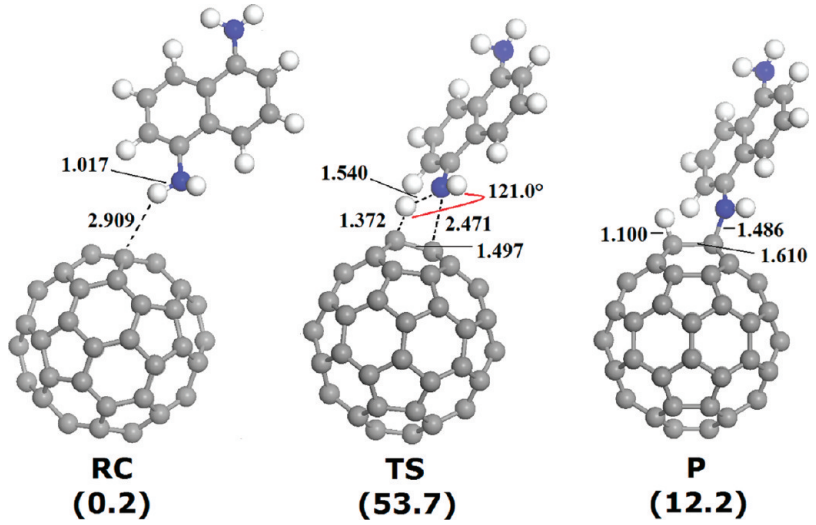

Figure 4. Optimized geometries for RC, TS, and P for the functionalization of fullerene C_{60} with DAN, as computed at the BLYP/DNP level of theory. Selected interatomic distances (in Ångstroms), angles (in degrees), and energies (in kcal mol^{-1}; relative to the level of isolated reactant species) are specified.

3 ns. The laser power was set to 80−90%. A pulsed ion extraction of 60−170 ns was employed to improve sensitivity.

Thermogravimetric analyses (TGA) were carried out on a Mettler Toledo 851e TGA/SDTA Instruments. Approximately 5 mg of powdered sample was heated in an open aluminum pan under air flow of 100 mL min^{-1}, with a heating ramp of 10 °C min^{-1} until 1000 °C. The curves recorded showed the weight loss (in mg) with simultaneous differential thermal analysis (SDTA).

Atomic force microscopy (AFM) images were obtained by using an Agilent 5500 multimode scanning probe microscope (Agilent Technologies, Inc., Chandler, AZ) with silicon cantilevers (Ted Pella, Inc., Redding, CA) operating in the intermittent-contact mode (AAC acoustic mode). Resonance frequencies of cantilevers were localized at approximately 300 kHz in the air. A typical scan rate for image acquisition was 1.0 line s^{-1} by using 512 × 512 pixel resolution. All samples were drop-casted onto Si/SiO_2 wafers and air-dried overnight in a desiccator prior to AFM measurements. Topographic image processing was performed by using PicoView 1.8.2 software.

4. RESULTS AND DISCUSSION

4.1. DFT Calculations. *Pure GGA-DFT Analysis.* The amination of fullerene C_{60} with methylamine has been previously studied within the framework of KS-DFT methods.[18,19] In the present study, the entire process for the gas-phase reaction $CH_3NH_2 + C_{60} \rightarrow C_{60}(H)NHCH_3$ (including reaction complex, transition state and products) was analyzed. The DFT-BLYP optimized structures of all stationary point geometries, that is, reaction complex (RC), transition state (TS), and product (P) are shown in Figure 1 with bond lengths in angstroms and bond angles in degrees. The respective data for ED, DAO, and DAN reactions sequences are depicted in Figures 2, 3, and 4. The calculated energies (in kcal mol^{-1}; relative to the level of isolated reactant species) of the optimized stationary point geometries are specified in Table 1.

At the BLYP/DNP level of theory, the interaction energies for the monoaddition of methylamine were calculated as −1.8 (RC), 75.4 (TS), and 4.6 (P) kcal mol^{-1}. At the PW91/DNP level, it has been reported[19] that the "reaction energy" for the

dx.doi.org/10.1021/jp211577k | J. Phys. Chem. A 2012, 116, 1663−1676

addition of methylamine on fullerene is −2.9 kcal mol^{-1}: apparently, this value corresponds to the energy of formation (relative to the level of isolated reactants CH_3NH_2 and C_{60}) of the monoadduct $C_{60}(H)NHCH_3$. We show the interaction energies computed with the BLYP, PW91, and PBE functionals in Table 1. For PW91 and PBE functionals, the energy of formation of $C_{60}(H)NHCH_3$ are −3.2 and −2.6 kcal mol^{-1}, respectively, which are very similar to the PW91/DNP value reported in ref 19, and probably the variation of 0.3 kcal mol^{-1} could be attributed to the chosen convergence threshold criteria. In our results, the difference observed between the PW91 (as well as PBE) and BLYP energies (∼7 kcal mol^{-1}) is not surprising because of the different behavior of the enhancement factor $F(s)$ in their respective $E_x[\rho]$ functionals. Specifically, functionals using the Becke approximation for exchange energy were shown to underestimate the forces in weakly bound systems, whereas the PW91 functional yield results comparable with MP2.[73,74] Moreover, the comparison between those pure GGA functionals also underlines the effect of the correlation functional (i.e., LYP performs much better than PW91 and PBE). Thus, there seems to be no relation of the overall functional performance to the value of the energy of product formation. Besides the use of KS-DFT methods is attractive in the realm of large systems, much care should be taken when applying DFT to molecular clusters where the dominant part of the stabilization energy comes from the dispersion energy; this energy contribution is not covered in the interaction energy (ΔE) which can lead to a large underestimation of the stabilization. The use of DFT for intermolecular interactions can be very deceptive,[75] especially when applying the variational supramolecular approach for computing ΔE_R (where R denotes RC, TS, or P) as a difference between the KS-DFT energy of an isolated complex (E_R) and the KS-DFT energies of isolated A and B reacting molecules that will form the complex: $\Delta E_R = E_R - (E_A + E_B)$. Within the framework of the variational supramolecular approach, the basis set inconsistency is the most serious obstacle and leads to the BSSE artifact. Unfortunately, the commercially available Material Studio Modeling 3.1 package does not allow for the BSSE correction. Therefore, we have calculated ΔE without the BSSE-corrected method and have to note that the final ΔE_R obtained (particularly for MA and ED amines) are rather qualitative. (For DAO and DAN amines, see the explanation in the following subsection.)

The calculated bonding energies for the noncovalent $CH_3NH_2\cdots C_{60}$ reaction complexes were found to be attractive, that is, −1.8 (BLYP), −2.6 (PW91), and −2.2 (PBE) kcal mol^{-1}. If one mainly considers equilibrium distances for common weakly bound complexes, PW91 provides at least qualitatively correct interaction potentials.[40] PBE produces attractive bonding energiy curves even for the rare-gas diatomic systems but exhibits an incorrect asymptotic behavior for large interatomic separation. Although even the pure GGA DFT-BLYP functional produces an attractive interaction in the reaction complex, it is not necessarily quantitatively accurate; one may attribute this behavior to the effectiveness of the numerical basis set employed.[63,76] While the whole process is endothermic by 6.4 kcal mol^{-1} for BLYP, the process turns be slightly exothermic by 0.6 and 0.4 kcal mol^{-1} for PW91 and PBE, respectively, relative to the RC level. Nevertheless, the activation energies ΔE_a (i.e., barriers separating reaction complex and products) are rather high for all the studied pure GGA functionals, that is, 77.3 (BLYP), 72.7 (PW91), and 73.6 (PBE) kcal mol^{-1}, thus indicating that the monoaddition reaction can thermodynamically be unfavorable. The high calculated transition state energies of more than 70 kcal mol^{-1} lead us to a conclusion that the gas-phase reaction $CH_3NH_2 + C_{60} \rightarrow C_{60}(H)NHCH_3$ never is energetically favorable at $T \rightarrow 0$. Following a simple Redhead's analysis of the migration temperature on solid surfaces,[77] we estimate the temperature necessary to overcome the energy barrier to be $T \approx 1200$ K ($\Delta E_a = 0.06\ T$ kcal mol^{-1} K^{-1}), which experimentally implies the decomposition of methylamine before it can react with C_{60}.

Despite of the calculations indicate that monoaddition of methylamine (i.e., the smallest organic amine) is unfeasible on C_{60}, this result does not contradict the experimental evidence available that fullerenes are readily aminated by more complex amines: for instance, *polyamines* (e.g., diethylenetriamine)[78] in solution or *long-chain monoamines* (e.g., nonylamine)[9] under the gas-phase conditions. This trend becomes evident by comparing the calculation results for MA and ED amines. As one can see from the values in Table 1, the calculated BLYP energies for the reaction $NH_2(CH_2)_2NH_2 + C_{60} \rightarrow C_{60}(H)$-$NH(CH_2)_2NH_2$ are −2.2 (RC), 71.8 (TS), and 4.6 (P) kcal mol^{-1}, which implies an endothermic process by 6.8 kcal mol^{-1} with respect to RC. On the contrary, the reaction turns slightly exothermic (by 0.1 kcal mol^{-1}) at the PW91/DNP and PBE/DNP levels of theory. Notably the activation energies are lower, especially for the case of the Perdew-type functionals, that is, 56.1 (PW91) and 56.3 (PBE) kcal mol^{-1} indicating that the monoaddition of ED onto C_{60} can thermodynamically be more favorable (by $T \approx 280$ K) than the addition of methylamine. From the above observations, one can anticipate that it is the long chain in amines which defines the decrease in activation energy for the amine addition reaction. As one can see in the case of DAO, the activation energies were computed as 42.8 (BLYP), 33.0 (PW91), and 33.2 (PBE) kcal mol^{-1}, which strongly supports our suggestion that the monoaddition reaction of large amines is thermodynamically more favorable than the addition of smaller amines. In the latter case, the reaction $NH_2(CH_2)_8NH_2 + C_{60} \rightarrow C_{60}(H)NH(CH_2)_8NH_2$ is predicted to be thermodynamically more favorable than the addition of MA (by $T \approx 665$ K) or ED ($T \approx 385$ K). As regards the aromatic DAN molecule, the computed activation barriers considerably decrease in this case as well, being 53.5 (BLYP), 44.5 (PW91), and 42.8 (PBE) kcal mol^{-1}.

For the reaction complexes (RCs), we analyzed the closest intermolecular distances, as well as the stretching vibration frequencies of N−H bonds of the diamine molecules. As shown in Figures 1−4, the reaction complexes are stationary points in which an amino hydrogen atom approaches the carbon atoms in the 6,6 junction of the pyracylene unit of C_{60}. In this way, the reaction complexes exhibit typical features in which the shortest distance $R{-}N(H)H\cdots C_{60}$ is ca. 3.0 Å, whereas the HN−H bond length is 1.02 Å. As regards harmonic vibration frequencies (nonscaled, calculated at the BLYP/DNP theoretical level), the most important characteristic absorption bands correspond to the stretching and scissoring N−H normal modes. The highest frequency band for RCs can be found in the spectra due to the antisymmetrical ν_{N-H} stretching mode, and which was calculated at 3862 (MA), 3844 (ED), 3812 (DAO), and 3843 cm^{-1} (DAN). The symmetrical ν_{N-H} stretching modes were calculated at 3778 (MA), 3733 (ED), 3696 (DAO), and 3742 cm^{-1} (DAN). Another very intensive band was attributed to the ν_{N-H} scissoring modes, whose calculated frequencies are 2477 (MA), 2372 (ED), 2377

dx.doi.org/10.1021/jp211577k | J. Phys. Chem. A 2012, 116, 1663−1676

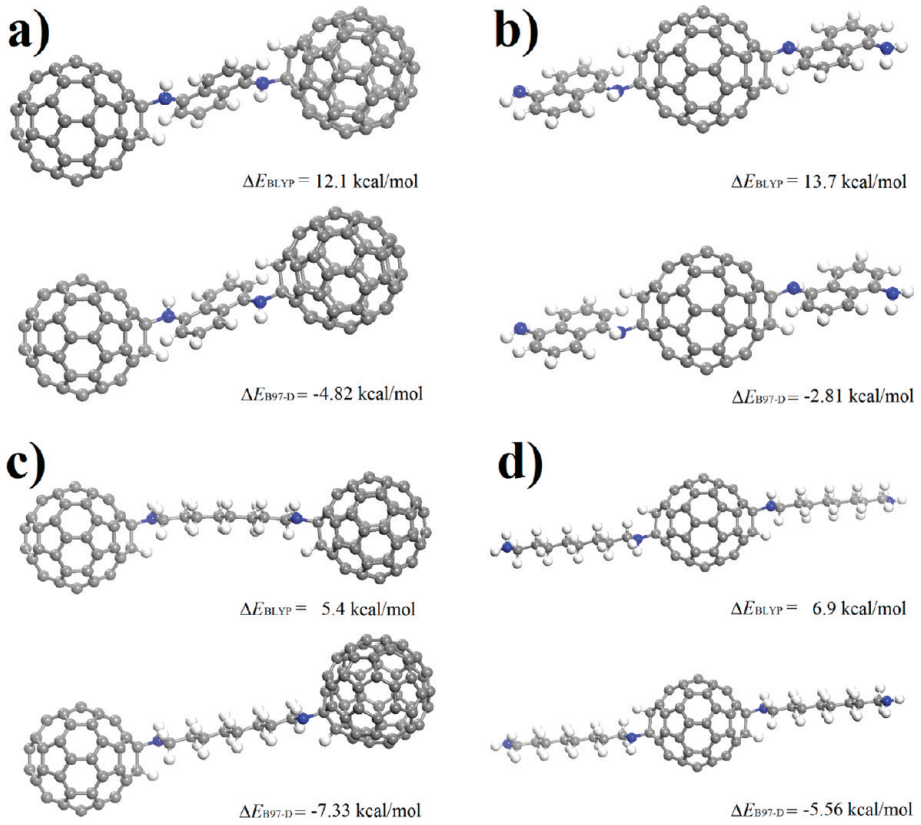

Figure 5. Optimized geometries of the products for the reaction between monoadducts and a second diamine molecule or fullerene cage: $(C_{60})_2$ + DAN (a); C_{60} + $(DAN)_2$ (b); $(C_{60})_2$ + DAO (c); C_{60} + $(DAN)_2$ (d). Relative BLYP and B97-D energies of formation (in kcal mol^{-1}) are specified.

(DAO), and 2158 cm^{-1} (DAN). Very small irregular variations (less than 10 cm^{-1}) in the calculated wavenumbers appear when using PW91 and PBE functionals; however, by comparing these values in the reaction complexes with those of isolated amine molecules, one can see a frequency shift by about 40−70 cm^{-1} apparently due to the fact that amines are influenced by a high electron density of fullerene.

From Figures 1−4, it becomes evident that the first addition of amine molecules requires overcoming the activation barrier of one transition state. Searches for transition states were carried out by using linear synchronous transit (LST) followed by a full conjugate gradient minimization method (LSTCG).[70] According to our results, TS structures indicate that the mechanism of reaction includes the coordination of one amino group to the 6,6 junction of pyracylene unit forming a four-membered ring, along with the transfer of one amine proton to a carbon atom in C_{60}. The most interesting feature in the TS geometries is the change in length of the 6,6 C−C bond in the pyracylene unit of fullerene, which is calculated as 1.403 Å for pristine fullerene with I_h symmetry. From the geometries shown, one can also see an increase in the C−C bond length for all TS structures, which is most significant for DAO (1.539 Å). Moreover, one can see that the resulting $RH_2N\cdots C_{60}$ separation for DAO is notably shorter (1.605 Å) as compared to the corresponding geometries for MA, ED and DAN (ca. 2.2 Å). A similar behavior is observed in the resulting HN···H separation (1.127 Å) as compared to ca. 1.5 Å for the other TSs formed with MA, ED, and DAN. The increased HN···H distance, preceding the loss of H, is compensated by increasing of the HN∠H angle (135° in MA and ED, 125° in DAO, and 121° in DAN) as compared to the typical values in pristine diamine molecules (106° in MA, ED, and DAO and 110° in DAN). All the transition states found exhibited only one imaginary frequency in their vibration spectra; the calculated absolute value for this frequency was approximately 750 cm^{-1} at the BLYP/DNP theoretical level.

The calculated ΔE values (see Table 1) show that the monoaddition reaction for DAO and DAN is an endothermic process, being at the same more favorable for DAO, whose molecules do not contain aromatic rings. Despite the higher dissociation energies associated with the rupture of N−H bonds compared to αC−H, the reaction mechanism described in Figures 1−4 supports the fact that the hydro-amination of fullerene C_{60} with primary amines favors the 1,2-addition pattern. The stationary point geometries of C_{60} + MA, C_{60} + ED, C_{60} + DAO, and C_{60} + DAN products are very similar to each other, in particular, the length of the C−C bond belonging to 6,6 junctions at the site where the 1,2-addition occurs, which is 1.60 Å. The highest frequency bands for the products are found in the calculated vibration spectra due to symmetrical ν_{N-H} stretching mode, with harmonic frequencies (nonscaled at the BLYP/DNP level of theory) of 3754 (C_{60} + MA), 3758 (C_{60} + ED), 3773 (C_{60} + DAO), and 3778 cm^{-1} (C_{60} + DAN).

As discussed, the calculated reaction energy for C_{60} + DAO and C_{60} + DAN products indicates an endothermic process as compared to the calculated exothermic process for their smaller counterparts MA and ED, which can apparently be explained by an increased steric hindrance in the case of DAO and DAN. While for methylamine, the polyaddition is exothermically favorable up to the penta adduct,[18] this can hardly be expected for such big molecules as DAO and DAN. Nevertheless, these long-chain amines can serve as sufficiently large spacers to make

dx.doi.org/10.1021/jp211577k | J. Phys. Chem. A 2012, 116, 1663−1676

feasible the cross-linking between two fullerene cages, a process which can be considered as alternative to a second diamine addition.

Semiempirical Dispersion GGA-DFT-D Analysis. Table 2 specifies the KS-DFT energies of formation of the two possible addition products (i.e., second diamine molecule by poly-addition pathway and a second fullerene molecule via cross-linking mechanism) obtained in the reactions of DAO and DAN with fullerene as calculated by using the pure GGA-DFT (BLYP, PW91, and PBE) and the semiempirical dispersion GGA-DFT-D (B97-D) functionals. Figure 5 compares the optimized geometries for the four possible products (two for DAO and two for DAN) as calculated by BLYP and B97-D functionals.

For the case of DAO, one can see that the pure GGA-DFT theory (BLYP) predicts the addition of two DAO molecules onto C_{60} to be less favorable than the formation of the cross-linked $(C_{60})_2$ + DAO product. Even in terms of the DFT-BLYP energies, for which an endothermic process was found, the cross-linked $(C_{60})_2$ + DAO product is not only more stable than C_{60} + DAO monoadduct (by 1.2 kcal mol^{-1}; for the corresponding PW91 and PBE energies this difference is around 1.6 kcal mol^{-1}) but also more stable than the diadduct C_{60} + $(DAO)_2$ by 1.5 (BLYP) and 1.7 (PW91 and PBE) kcal mol^{-1}. In the case of the aromatic diamine DAN, the $\Delta\Delta E$ formation energies (which are relative to C_{60} + DAN monoadduct) indicate that the cross-linked fullerene $(C_{60})_2$ + DAN is energetically favored by −0.1 (BLYP), −0.4 (PW91), and −0.6 (PBE) kcal mol^{-1}. Similarly to the reaction with DAO, the addition of two DAN molecules onto C_{60} turns out to be thermodynamically less favorable as compared to the cross-linking mechanism ($\Delta\Delta E$ = 1.5 kcal mol^{-1}); this might be associated with the rigid aromatic structure of DAN molecule. In this way, the overall results of pure GGA-DFT calculations suggest that both $(C_{60})_2$ + DAO and $(C_{60})_2$ + DAN cross-linked products are thermodynamically more favorable as compared to the C_{60} + amine monoadducts. Furthermore, according to the $\Delta\Delta E$ values calculated by pure GGA-DFT, it appears that the cross-linking mechanism is preferred in the reaction between the aliphatic long-chain diamine DAO and C_{60}.

Further validation calculations were performed using the semiempirical dispersion GGA B97-D functional. The formation energies for the diaddition and cross-linked products as calculated at the B97-D/6-31G(*d*,*p*) level of theory are given in Table 2. Because of dispersion inclusion into the B97-D method, we observed that the main difference with respect to the pure GGA-DFT methods is that all the calculated formation energies predict exothermic processes, even in the case of C_{60} + DAO and C_{60} + DAN monoadducts for which all the pure GGA-DFT methods predicted endothermic processes. In terms of the formation energies, the numerical difference between pure GGA-DFT and semiempirical B97-D values is noticeably larger; in particular, by comparison of the BLYP and B97-D energies we observed a large difference that exceeds 15.0 kcal mol^{-1}. Interestingly, there are not significant differences between the B97-D and the corresponding B97-D ZPE-corrected energies; on average, the ZPE contribution to the total DFT-D energy is ca. 0.2 kcal mol^{-1}. We attribute this effect to an autocancellation of numerical errors in the DFT-D calculations of the energies of formation. As noted by Grimme,[52,54] the DFT-D ΔE values are not BSSE-corrected, and thus semiempirical dispersion DFT-D calculations provide a good accuracy even without correcting for BSSE when reasonably polarized triple-ζ basis set are applied (e.g., TZV(2df,2pd)). In particular, in a large benchmark set of 161 base pairs, amino acid pairs, and other small complexes,[79] the statistic root-mean-square deviation between B97-D/TZV-(2df,2pd) level of theory and reference ΔE values was reported to be 0.92.

With concern for the diaddition and cross-linking mechanisms considered here, the B97-D energies indicate that both C_{60} + $(DAO)_2$ and C_{60} + $(DAN)_2$ diaddition products turn out to be less favorable with respect to the corresponding C_{60} + DAO and C_{60} + DAN monoadducts. Nevertheless, the calculated energies indicate exothermic formation for both cross-linked and diadduct products, for both DAO and DAN. In particular, the formation of C_{60}+$(DAO)_2$ is viable since its process was calculated as exothermic by ca. 5.6 kcal mol^{-1} (ca. 4.0 kcal mol^{-1} ZPE-corrected). Similarly, the formation of C_{60} + $(DAN)_2$ is exothermic by ca. 2.8 kcal mol^{-1} (ca. 1.6 kcal mol^{-1} B97-D ZPE-corrected). On the basis of the calculated DFT-D energies, the alternative cross-linking mechanism is more favorable in the case of aromatic DAN, for which the $(C_{60})_2$ + DAN formation is more exothermic with respect to both C_{60} + DAN (by 0.2 kcal mol^{-1}) and C_{60} + $(DAN)_2$ (by 2.0 kcal mol^{-1}); on the other hand, in terms of the B97-D (ZPE) values this difference turns to be insignificant (∼0.1 kcal mol^{-1}). This suggests that treating fullerene C_{60} with diamines—under the gas-phase reaction conditions—would produce a mixture of monoadducts, diadducts, and probably other polyadducts, along with cross-linked species.

The general performance of all pure GGA-DFT functionals tested here reflects the well-known lack of adequately description of dispersive energies. As a whole, the processes are predicted as thermodynamically unfavorable when using pure GGA-DFT methods. Particularly, BLYP yields the worst results by yielding "repulsive" energies, and it cannot be recommended for reaction characterization (ΔE energies for RC, TS, or P), especially because of the need for BSSE correction. Figure 5 shows the optimized geometries and formation energies for the cross-linked $(C_{60})_2$ + DAN and $(C_{60})_2$ + DAO and diaddition C_{60} + $(DAN)_2$ and C_{60} + $(DAO)_2$ species (the orientation of the fullerene cage was intended to keep the same with respect to the pyracylene units reacted). The most dramatic effect of the inclusion of dispersion contribution was observed for $(C_{60})_2$ + DAO and C_{60} + $(DAO)_2$ species. There are notable differences between pure GGA-DFT and GGA-DFT-D geometries in the case of $(C_{60})_2$ + DAO, specifically in the aliphatic chain connecting the two fullerene cages. Here, the C−C bond length and the HC∠H angle calculated with BLYP are respectively longer by ca. 0.03 Å and lower by 0.3° as compared to the values obtained with semiempirical dispersion GGA-DFT-D functional. Because of a significantly different exchange contribution, PW91 and PBE functionals perform better and might be used after BSSE correction. The B97-D results apparently better much the available experimental data (which will be discussed below).

Frontier Molecular Orbital Analysis. To briefly characterize the electronic properties of C_{60} + amine addition products, we also calculated the highest-occupied molecular orbital (HOMO)−lowest-unoccupied molecular orbital (LUMO) gap values in the frame of the time-independent KS-DFT formalism. As obtained with pure GGA-DFT and semiempirical GGA-DFT-D methods, the electronic HOMO−LUMO gap energies, ΔE_{gap}, of the C_{60} + DAO and C_{60} + DAN species are

Table 3. Electronic HOMO−LUMO Gap Energies ΔE_{gap} (in eV) as Calculated with the Pure GGA BLYP, PW91, and PBE Functionals (in Conjunction with the DNP Basis Set) and with the Semiempirical Dispersion GGA B97-D Functional (in Conjunction with the 6-31G(d,p) Basis Set)[a]

	GGA-DFT						GGA-DFT-D	
system	BLYP	$\Delta\Delta E_{gap}$	PW91	$\Delta\Delta E_{gap}$	PBE	$\Delta\Delta E_{gap}$	B97-D	$\Delta\Delta E_{gap}$
C_{60} + DAO	1.336		1.218		1.231		1.485	
$(C_{60})_2$ + DAO	1.478	0.14	1.478	0.26	1.476	0.25	1.602	0.12
C_{60} + $(DAO)_2$	1.406	0.07	1.375	0.16	1.389	0.16	1.413	− 0.07
C_{60} + DAN	0.570		0.553		0.550		0.663	
$(C_{60})_2$ + DAN	0.673	0.10	0.665	0.11	0.654	0.10	0.793	0.13
C_{60} + $(DAN)_2$	0.574	0.00	0.552	0.00	0.549	0.00	0.687	0.02
DAO	6.356		6.544		6.554		6.802	
DAN	2.896		2.921		2.919		2.939	
C_{60}[b]	1.664		1.672		1.671		1.673	

[a]Relative $\Delta\Delta E_{gap}$ energies (in eV) are shown with respect to the C_{60} + diamine monoadducts. [b]Fullerene at the symmetry I_h point group.

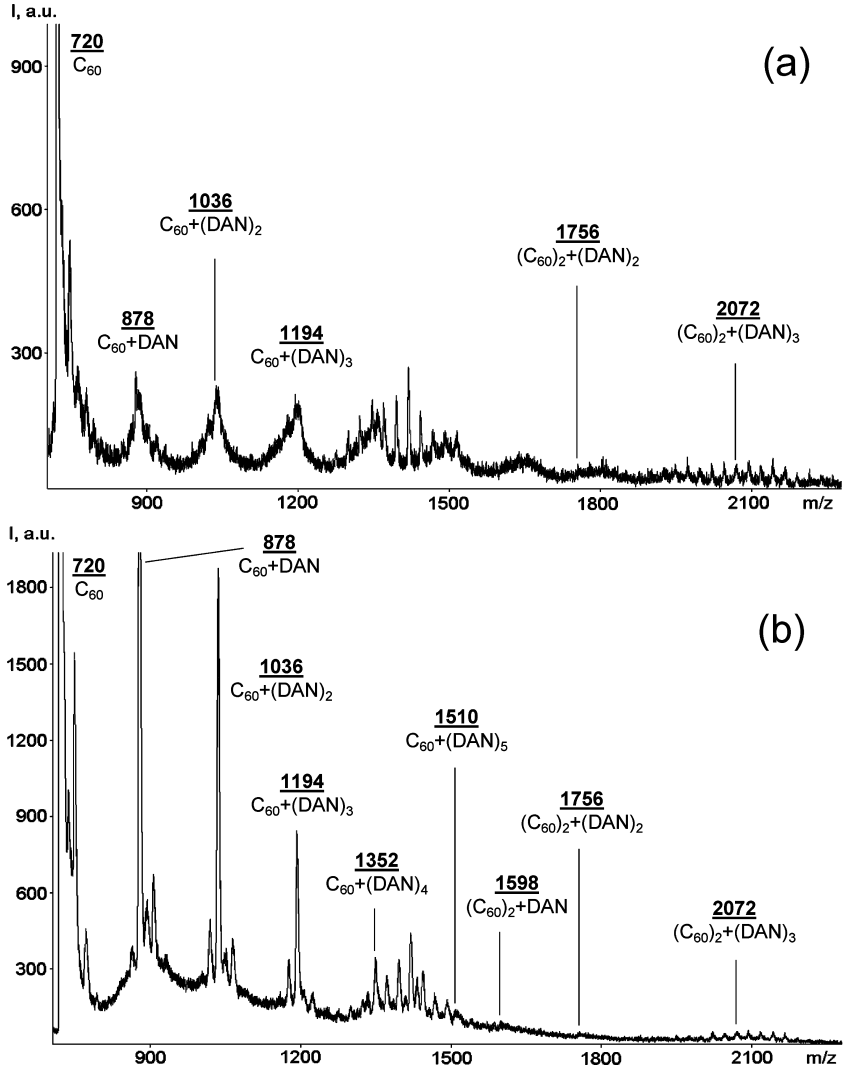

Figure 6. Representative positive (a) and negative ion (b) LDI-TOF mass spectra of DAN-functionalized fullerene C_{60}.

given in Table 3. Because of the fact that the frontier molecular orbital eigenvalues are generally insensitive to the basis set employed,[80] we did not test basis sets other than DNP in the case of pure GGA-DFT methods. The Kohn−Sham eigenvalues are just the starting points to compare the electronic properties of isolated molecules. Most approximate theories (such as the time-dependent DFT[81]) yield more realistic results; however, one can appeal to the time-independent KS-DFT calculations to qualitatively understand the stability of the proposed C_{60} + amine species, bearing in mind that the reactions between fullerene and amines are mostly of low selectivity and yield complex mixtures of several products.

As one can expect, both C_{60} + DAO and C_{60} + DAN monoadducts would preferentially react with molecules whose

dx.doi.org/10.1021/jp211577k | J. Phys. Chem. A 2012, 116, 1663−1676

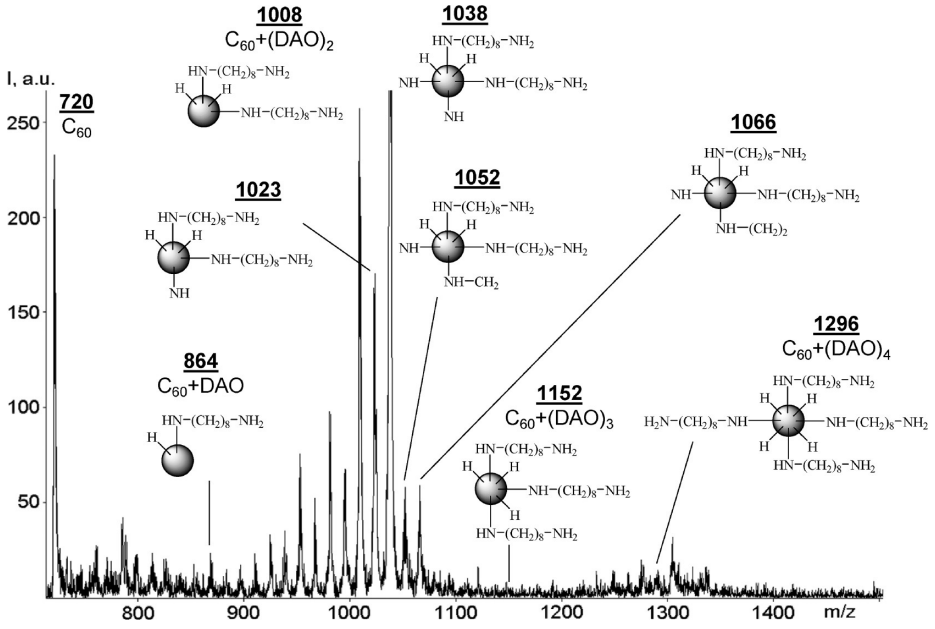

Figure 7. Representative negative ion LDI-TOF mass spectra of DAO-functionalized fullerene C_{60}. Fullerene cages are shown as balls for convenience.

frontier orbitals are closest in energy to their own. More precisely, if these molecules act as nucleophiles then they will react with electrophiles having the lowest LUMO energies. In particular, at the B97-D/6-31G(d,p) level of theory, the HOMO energies for C_{60} + DAO (E_{HOMO} = −5.054 eV) and C_{60} + DAN (E_{HOMO} = −4.276 eV) monoadducts indicate that such species preferentially will react with fullerene (E_{LUMO} = −3.705 eV) to form the respective cross-linked products $(C_{60})_2$ + DAO and $(C_{60})_2$ + DAN, whose formation is exothermic processes, being more favorable in the case of DAN (Table 2). The calculated LUMO energies for DAO and DAN are 1.797 and −1.079 eV, respectively.

It is well-known that molecular systems having large ΔE_{gap} values are more stable and chemically unreactive than those having smaller gap values. As a whole, from the ΔE_{gap} values reported in Table 3, one can see that both pure DFT and semiempirical DFT-D functionals predict all the C_{60} + amine species to be chemically more reactive with respect to pristine fullerene ($\Delta E_{gap} \approx 1.67$ eV) as well as to isolated DAO ($\Delta E_{gap} \approx 6.5$ eV) and DAN ($\Delta E_{gap} \approx 2.9$ eV). The chemical reactivity is most notorious for C_{60} + DAN adduct whose HOMO−LUMO gap values were calculated around 0.6 eV; for C_{60} + DAO species, the HOMO−LUMO gap values are almost 1.4 eV. The latter result suggests that the improved photovoltaic performance achieved by the functionalization of C_{60} with aromatic DAN would not depend on the product type, that is, whether it is polyadduct or cross-linked species. By comparing the $\Delta\Delta E_{gap}$ energies (relative to C_{60} + amine monoadducts) for the cross-linked and diaddition products, we observe only a small difference ($\Delta\Delta E_{gap} < 0.1$ eV) which means that such products have a similar stability. Still, the cross-linked products are slightly more stable, and one can rationalize that some degree of covalent cross-linking is required to reduce the gap of pristine fullerene material in the development of novel bulk organic heterojuntions.

4.2. LDI-TOF Mass Spectra. LDI-TOF mass spectrometry is one of very few analytical techniques capable to give an insight into the diamine addition pathways and to experimentally complement our theoretical models. In a particular case of DAN, we were able to obtain good-quality mass spectra of both negative and positive ions, which are shown in Figure 6. In the representative (both positive and negative ion) spectra, one can clearly identify a number of addition products of variable fullerene:DAN stoichiometry, namely 1:1 (m/z 878), 1:2 (m/z 1036), 1:3 (m/z 1194), 1:4 (m/z 1352), 1:5 (m/z 1510), 2:1 (m/z 1598), 2:2 (m/z 1756) and 2:3 (m/z 2072). The first five peaks along with their high intensities strongly favor the reaction preference toward diamine polyaddition to a single fullerene cage. This finding correlates very well with our earlier theoretical calculations for the methylamine reactions with C_{60}, where amine polyaddition was found to be favorable up to the formation of penta-adduct.[18] At the same time, the cross-linking pathway evidently takes place as well, as supported by the presence of smaller peaks due to $(C_{60})_2$ + DAN, $(C_{60})_2$ + $(DAN)_2$, and $(C_{60})_2$ + $(DAN)_3$. Other peaks in these LDI-TOF mass spectra can correspond to fragments of some (or all) adducts mentioned above as well as to higher-molecular-weight products (especially the peaks with m/z higher than 2072 amu of $(C_{60})_2$ + $(DAN)_3$).

In the case of DAO addition to fullerene, positive ion mass spectra turned to be of poor quality (therefore not shown), contrary to negative ion mass spectra exemplified by the one presented in Figure 7. Like for DAN adducts, we identified a series of addition products of variable fullerene:DAO stoichiometry, such as 1:1, 1:2, 1:3, and 1:4. (Again, this result correlates well with our earlier theoretical calculations for the methylamine polyaddition onto C_{60}, which is favorable up to the formation of penta-adducts.[18]) A large number of peaks correspond to fragment ions originating from the DAO polyaddition products. The character of fragmentation can be illustrated by the structures corresponding to m/z 1023, 1038, 1052, and 1066. All of them most likely originate from triadduct C_{60} + $(DAO)_3$ and tetra-adduct C_{60} + $(DAO)_4$, which undergo the cleavage of one or more DAO chains at different sites, with the loss of amino alkyl radicals. At the same time, no evident peaks pointing to the formation of cross-linked

dx.doi.org/10.1021/jp211577k | J. Phys. Chem. A 2012, 116, 1663−1676

fullerene cages were detected, which strongly suggests that the polyaddition pathway is strongly favored in the case of DAO, in agreement with the theoretical B97-D results.

4.3. TGA. TGA results are depicted in Figure 8 for pristine fullerene C_{60} (a) as well as for C_{60} reacted with DAO (b) and DAN (c). As expected, the TGA curves show significant differences in the behavior of amine-functionalized products and pristine fullerene. Pristine C_{60} shows uniform weight decrease after 500 °C down to total decomposition at 770 °C; this result is consistent with our previous TGA data[9] on predried fullerene samples. In addition, the SDTA curve shows almost three exothermic events, in which the temperature of the maximum rate of oxidation of pure C_{60} is 629 °C. The possibility of adsorbing some impurities from air is a likely reason for the appearance of a minor peak at 496 °C. As regards the third (also smaller than the main one) peak at 763 °C, it is likely due to the decomposition of primary products of thermal transformations of starting C_{60} due to its oxidation, polymerization, etc.

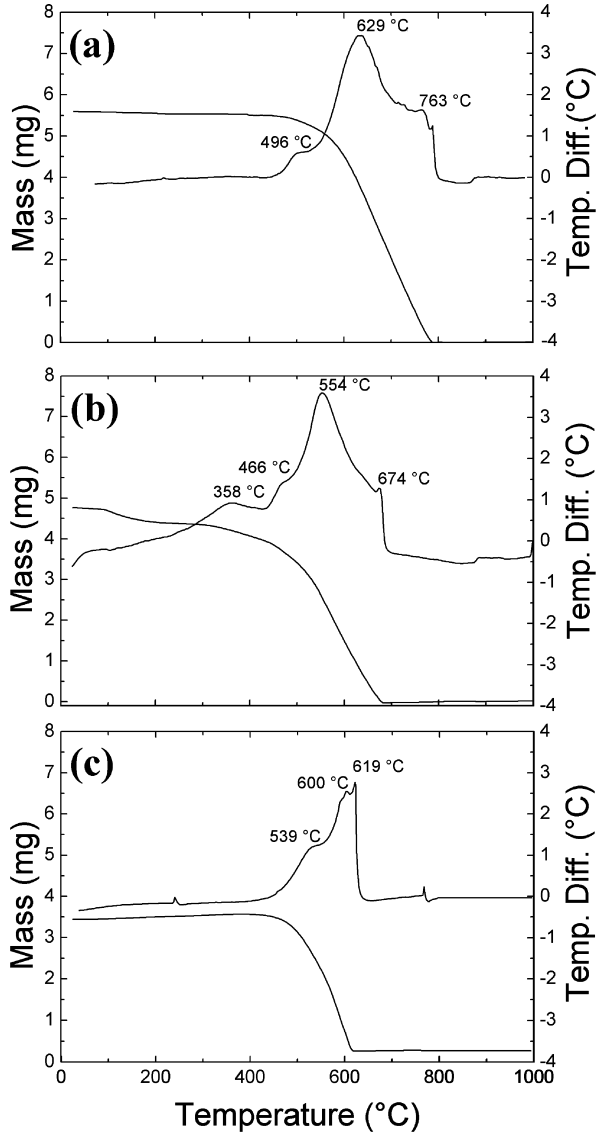

Figure 8. TGA curves for a sample of pristine fullerene C_{60} (a) and for C_{60} reacted with DAO (b) and DAN (c). SDTA curves show exothermic events; heating rate is 10 °C/min in air.

It is evident that the process of decomposition for C_{60} reacted with DAO and DAN proceeds in different ways. While the sample of C_{60} treated with DAN exhibits in TGA only one sharp and uniform weight loss after ca. 500 °C (Figure 8c), for C_{60} treated with DAO (Figure 8b) the decomposition is stepwise: the first weight loss is of a few percent up to 100 °C, then two steps of weight loss of <20 wt % between 100 and 300 °C, and then between 300 and 420 °C, followed by complete gradual decomposition of the sample around 670 °C. One cannot discard the possibility that the weight loss in the temperature interval of 100−300 °C might correspond to DAO molecules physisorbed on and between fullerene cages in crystalline C_{60} because of strong hydrophobic interactions, similar to the phenomenon observed in the functionalization of carbon nanotubes with amines.[28,29] The remaining weigh loss between 300 to 420 °C might correspond to the initial decomposition of DAO moieties covalently attached to fullerene (apparently more than one covalently linked DAO molecule per one fullerene cage, as shown by LDI-TOF mass spectra). Unfortunately, it is impossible to estimate by TGA the contribution of amine species covalently bound and physisorbed onto fullerene. At the same time, the simultaneously measured SDTA curves show the maximum rate of oxidation around 550 °C for C_{60} reacted with DAO and 600 °C for C_{60} reacted with DAN, and therefore are indicative of considerably higher resistance to oxidative decomposition for C_{60} reacted with DAN than for C_{60} reacted with DAO. The latter result is consistent with the proposed cross-linking mechanism, which contributes in the case of aromatic amine addition. Logically one can expect that the greater the number of cross-linked units in the composites the more resistant the bulk material will be to thermal degradation.

4.4. AFM Measurements. Figure 9 shows AFM topography images of the experimentally obtained fullerene C_{60} samples functionalized with DAO and DAN by means of the solvent-free gas-phase technique. Here one can observe aggregation of the functionalized materials, in whose structure it is impossible to distinguish single fullerene molecules. At the same time, there are clear differences in the degree of aggregation, depending on whether the aliphatic (DAO) or aromatic (DAN) diamines were employed. These differences are better seen at a higher magnification, at the right-hand images (see parts b and d of Figure 9). While the functionalization with aliphatic DAO leads to a more homogeneous structure, the functionalization with aromatic DAN produces larger aggregates seen as islands of ca. 500 nm in diameter, more separated from each other. Possible reasons for the differences observed are: different degree of polyaddition/cross-linking reactions, and correspondingly different molecular weight of the final products; stronger adhesion between smaller structural units in the case of DAN, due to the stacking effects intrinsic to the aromatic DAN molecules; etc.

The AFM topography of the C_{60} + diamine composites also can be explained in terms of the theoretical models studied, namely, by the strength of interactions between the aliphatic vs aromatic diamine molecules and fullerene cage (see Table 2; B97-D results). In particular, we calculated that the monoaddition of DAO onto fullerene is a process exothermically more favorable (by ca. 2.7 kcal mol^{-1}) than the addition of the DAN molecule. Moreover, the second addition of DAO (i.e., C_{60} + $(DAO)_2$) is also a process thermodynamically favored by ca. 2.7 kcal mol^{-1} as compared to the second

dx.doi.org/10.1021/jp211577k | J. Phys. Chem. A 2012, 116, 1663−1676

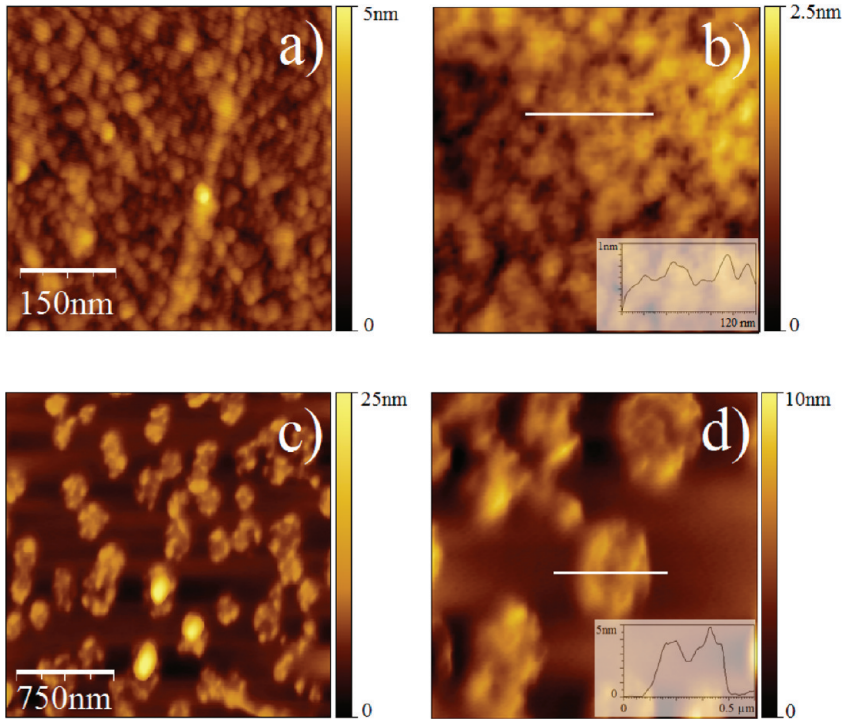

Figure 9. (a) AFM topography images of DAO-functionalized fullerene C_{60} (z scale: 0−5.0 nm) and (b) magnification image (area size 350 × 350 nm^2, scan speed 1.0 line s^{-1}) showing a cross section along the white line indicated (120 nm). (c) AFM topography images of DAN-functionalized fullerene C_{60} (z scale: 0−25.0 nm) and (d) magnification image (area size 1.2 × 1.2 μm^2, scan speed 1.0 line s^{-1}) showing a cross section along the white line indicated (500 nm).

addition of DAN. Therefore, one can expect that the final degree of functionalization with aliphatic DAO will be higher, resulting in the formation of more amorphous products with a higher molecular weight, which are more uniformly distributed at the AFM supports (in our particular case Si/SiO_2 wafers).

In a recent study,[32] we showed that the functionalization of multiwalled carbon nanotubes with DAO produces micrometer-sized structures, indicative of a high degree of interconnection between the functionalized nanotubes; in other words, this result implies that DAO molecules can efficiently act as covalent linkers between nanotubes. According to the images from Figure 9, the structure of DAO-functionalized fullerene matrial is comparatively "smoother", of no more than 3 nm in height. This can be interpreted as the functionalization with the aliphatic diamine DAO can be more suitable to produce continuous uniform structures (e.g., nanosized layers or films), where no major defects (such as protrusions, holes, rifts, agglomerates, etc.) are observed. On the other hand, we recently demonstrated[11] that the gas-phase treatment with aromatic DAN is an efficient way for functionalizing *prefabricated* thin films of C_{60}; the functionalized materials exhibit lower surface roughness, supporting the fact that the diamine molecules might be able to penetrate throughout the entire fullerene solid phase in the film. In the present case, the aggregates evident in parts c and d of Figure 9 are not interconnected with each other because the degree of polyamination/cross-linking is apparently low—possibly due to the more rigid character of aromatic DAN molecule. The mechanism of aggregation of DAN-functionalized fullerene can be envisioned as the consequence of electrostatic interactions; that is, the aromatic DAN molecules induce electrostatic forces due to which local small individual aggregates form once DAN-functionalized fullerene is deposited onto the Si/SiO_2 supports for AFM. Since these aggregates can be formed by smaller clusters, the resulting structure is notably inhomogeneous, where different cluster diameters can be measured; their heights are generally not more than 10 nm.

5. CONCLUSIONS

The products of amine addition to fullerene C_{60} were theoretically studied using KS-DFT methodologies, and experimentally analyzed employing LDI-TOF mass spectrometry, TGA, and AFM techniques. The entire chemical process was studied using the pure GGA BLYP, PW91, and PBE functionals. In terms of pure GGA-DFT energies, the monoaddition reactions are generally unfavorable since, in a number of cases, endothermic processes were predicted. Notably, the activation energies were found to be lower for the Perdew-type functionals, indicating that the monoaddition of long-chain amines (e.g., DAO) is thermodynamically more favorable than the addition of smaller amines (e.g., MA and EN). A second reaction of DAO and DAN with fullerene molecule might produce the cross-linked species $(C_{60})_2$ + DAO and $(C_{60})_2$ + DAN; their formation was calculated to be an exothermic process, being somewhat more favorable in the case of DAN. Further validation calculations for the DAO and DAN reactions were carried out using the semiempirical dispersion GGA B97-D functional. In terms of the DFT-D formation energies, all the reactions are predicted to be exothermic and thus favorable, at the same time suggesting that the cross-linked products $(C_{60})_2$ + DAO and $(C_{60})_2$ + DAN are thermodynamically more stable than their respective diadducts (by ca. 1.7 kcal mol^{-1}) and monoadducts. According to the frontier molecular orbital analysis, the chemical reactivity is most notorious for C_{60} + DAN whose HOMO−LUMO gap energies calculated were around 0.6 eV; for C_{60} + DAO, HOMO−LUMO gap energies

dx.doi.org/10.1021/jp211577k | J. Phys. Chem. A 2012, 116, 1663−1676

are almost 1.4 eV. Experimentally, LDI-TOF mass spectrometry confirms the addition reactions of diamines with C_{60}, which can take place through either polyaddition or cross-linking pathways. While the polyaddition (of up to four diamine molecules) process turns to be preferable with DAO, in the case of DAN we observed that the cross-linking pathway is possible as well, as supported by peaks due to $(C_{60})_2$ + DAN, $(C_{60})_2$ + $(DAN)_2$, and $(C_{60})_2$ + $(DAN)_3$. TGA and SDTA analysis showed significant differences between the curves of the diamine-functionalized samples and pristine fullerene. AFM topography images suggested that the fullerene functionalization with DAO and DAN leads to oligomeric or polymeric materials; apparently, the functionalization with aliphatic diamines is more useful to produce continuous and homogeneous surface structures (e.g., nanosized layers and films). The results obtained might be useful to open a new route to amino-functionalized fullerene-based conductive lightweight materials, such as fullerene-grafted polymers and highly cross-linked amino-fullerenes.[16]

AUTHOR INFORMATION

Corresponding Author

*Phone: (+52) 55 56 22 86 02, ext. 1150. E-mail: flavioc@nucleares.unam.mx.

Notes

The authors declare no competing financial interest.

ACKNOWLEDGMENTS

Financial support from the National Autonomous University of Mexico (Grant No. DGAPA-IN100610), from the National Council of Science and Technology of Mexico (CONACyT, Grant No. 127299), and from the Institute of Science and Technology of the Federal District Government (Grant No. ICyTDF 333/2009) is greatly appreciated. F.F.C.-T. acknowledges support from the Institute of Science and Technology of the Federal District Government, ICyTDF, for a postdoctoral fellowship (contract ICYTDF/SRI/2/2011). V.A.B. and E.V.B. thank DGAPA UNAM for supporting their sabbatical stay at the University of Turin. We also thank the Supercomputing Department of DGTIC-UNAM for computer resources, in particular Leobardo Itehua for his technical assistance and Juan Rizo for assistance in TGA measurements.

REFERENCES

(1) Dresselhaus, M. S.; Dresselhaus, G.; Elkund, P. C. *Science of Fullerenes and Carbon Nanotubes*; Academic Press, 1996.
(2) Alvarez-Zauco, E.; Sobral, H.; Basiuk, E. V.; Saniger-Blesa, J. M.; Villagrán-Muniz, M. *Appl. Surf. Sci.* **2005**, *248*, 243−247.
(3) Talyzin, A. V.; Dubrovinsky, L. S.; Le Bihan, T.; Jansson, U. *Phys. Rev. B* **2002**, *65*, 245413.
(4) Yogo, A.; Majima, T.; Itoh, A. *Nucl. Instrum. Methods Phys. Res. B* **2002**, *193*, 299−304.
(5) Basiuk (Golovataya-Dzhymbeeva), E. V.; Alvarez-Zauco, E.; Basiuk, V. A. *Micromanufacturing and Nanotechnology*; Mahalik, N., Ed.; Springer-Verlag, Berlin, 2005; pp 453−461.
(6) Bao, Z.; Lovinger, A. J.; Brown, J. *J. Am. Chem. Soc.* **1998**, *120*, 207−208.
(7) Katz, H. E.; Johnson, J.; Lovinger, A. J.; Li, W. *J. Am. Chem. Soc.* **2000**, *122*, 7787−7792.
(8) Chen, H. Z.; Ling, M. M.; Mo, X.; Shi, M. M.; Wang, M.; Bao, Z. *Chem. Mater.* **2007**, *19*, 816−824.
(9) Basiuk (Golovataya-Dzhymbeeva), E. V.; Basiuk, V. A.; Shabel'nikov, V. P.; Golovatyi, V. G.; Flores, J. O.; Saniger, J. M. *Carbon* **2003**, *41*, 2339−2346.
(10) Dmitruk, N. L.; Borkovskaya, O.Yu.; Manontova, I. B.; Kondratenko, O. S.; Naumenko, D. O.; Basiuk (Golovataya-Dzhymbeeva), E. V.; Alvarez-Zauco, E. *Thin Solid Films* **2007**, *515*, 7716−7720.
(11) Martínez-Lorán, E.; Alvarez-Zauco, E.; Basiuk, V. A.; Basiuk, E. V.; Bizarro, M. *J. Nanosci. Nanotech.* **2011**, *11*, 5569−5573.
(12) Chiba, K.; Ohsaka, T.; Ohnuki, Y.; Oyama, N. *J. Electroanal. Chem.* **1987**, *219*, 117−124.
(13) Oyama, N.; Sato, M.; Ohsaka, T. *Synth. Met.* **1989**, *29*, E501−E506.
(14) Jackowska, K.; Bukowska, J.; Jankowski, M. *J. Electroanal. Chem.* **1995**, *388*, 101−108.
(15) Ishimaru, S.; Yamauchi, M.; Ikeda, R. *Solid State Commun.* **2003**, *127*, 57−59.
(16) Miller, G. P. *C. R. Chim.* **2006**, *9*, 952−959.
(17) Lee, J.; Mackeyev, Y.; Cho, M.; Wilson, L. J.; Kim, J.-H.; Alvarez, P. J. J. *Environ. Sci. Technol.* **2010**, *44*, 9488−9495.
(18) Amelines-Sarria, O.; Basiuk, V. A. *J. Comput. Theor. Nanosci.* **2009**, *6*, 73−79.
(19) Lin, T.; Zhang, W. D.; Huang, J.; He, C. *J. Phys. Chem. B* **2005**, *109*, 13755−13760.
(20) Amelines-Sarria, O.; Basiuk, V. A. *Superlattices Microstruct.* **2009**, *46*, 302−305.
(21) Meador, M. A. B.; Fabrizio, E. F.; Ilhan, F.; Dass, A.; Zhang, G.; Vassilaras, P.; Johnston, J. C.; Leventis, N. *Chem. Mater.* **2005**, *17*, 1085−1098.
(22) Nigam, A.; Shekharam, T.; Bharadwaj, T.; Giovanola, J.; Narang, S.; Malhotra, R. *J. Chem. Soc., Chem. Commun.* **1995**, 1547−1549.
(23) Wuld, F.; Hirsch, A.; Khemani, K. C.; Suzuki, T.; Allemand, P.-M.; Koch, A.; Eckert, H.; Srdanov, 0.; Webb, H. M. *ACS Symp. Ser.* **1992**, *481*, 161−175.
(24) Meza-Laguna, V.; Basiuk, E. V.; Alvarez-Zauco, E.; Gromovoy, T.Yu.; Amelines-Sarria, O.; Bassiouk, M.; Puente-Lee, I.; Basiuk, V. A. *J. Nanosci. Nanotech* **2008**, *8*, 3828−3837.
(25) Meza-Laguna, V.; Basiuk, E. V.; Alvarez-Zauco, E.; Acosta-Najarro, D.; Basiuk, V. A. *J. Nanosci. Nanotech.* **2007**, *7*, 3563−3571.
(26) Basiuk, E. V.; Puente-Lee, I.; Claudio-Sánchez, J.-L.; Basiuk, V. A. *Mater. Lett.* **2006**, *60*, 3741−3746.
(27) Basiuk, V. A.; Salvador-Morales, C.; Basiuk, E. V.; Jacobs, R. M. J.; Ward, M.; Chu, B. T.; Sim, R. B.; Green, M. L. H. *J. Mater. Chem.* **2006**, *16*, 4420−4426.
(28) Basiuk, E. V.; Gromovoy, T.Yu.; Datsyuk, A. M.; Palyanytsya, B. B.; Pokrovskiy, V. A.; Basiuk, V. A. *J. Nanosci. Nanotech.* **2005**, *5*, 984990.
(29) Basiuk, E. V.; Basiuk, V. A.; Bañuelos, J.-G.; Saniger-Blesa, J.-M.; Pokroskiy, V. A.; Gromovoy, T. Yu.; Mischanchuk, A. V.; Mischanchuk, B. G. *J. Phys. Chem. B* **2002**, *106*, 1588−1597.
(30) Haddon, R. C. *Science* **1993**, *261*, 1545−1550.
(31) Contreras-Torres, F. F.; Basiuk, V. A.; Basiuk, E. V. *J. Phys. Chem. A* **2008**, *112*, 8154−8163.
(32) Contreras-Torres, F. F.; Ochoa-Olmos, O. E.; Basiuk, E. V. *J. Scanning Probe Microsc.* **2009**, *4*, 100−106.
(33) Parr, R.; Yang, W. *Density Functional Theory of Atoms and Molecules*; Oxford University Press: New York, 1989.
(34) Hohenberg, P.; Kohn, W. *Phys. Rev.* **1964**, *136*, B864−B871.
(35) Kohn, W.; Sham, L. J. *Phys. Rev.* **1965**, *140*, A1133−A1138.
(36) Perdew, J. P.; Schmidt, K. *Jacob's ladder of Density Functional Approximations for the Exchange-Correlation Energy*; AIP: New York, 2001; Vol. *577*.
(37) Perdew, J.; Kurth, S. *A Primer in Density Functional Theory*; Springer Verlag: Berlin Heidelberg, 2003.
(38) (a) Jones, R. O.; Gunnarsson, O. *Phys. Rev. Lett.* **1985**, *55*, 107−110. (b) Gunnarsson, O.; Jones, R. O. *Phys. Rev. B* **1985**, *31*, 7588−7602.
(39) Strictly, the dispersion interaction is defined in the asymptotic region only, and the terminology becomes ambiguous when molecular densities overlap.
(40) Grimme, S. *WIREs Comput. Molec. Sci.* **2011**, *1*, 211−228.
(41) Perdew, J. P.; Zunger, A. *Phys. Rev. B* **1981**, *23*, 5048−5079.

(42) Becke, A. D. *J. Chem. Phys.* **1993**, *98*, 1372−1377.
(43) Frydel, D.; Terilla, W. M.; Burke, K. *J. Chem. Phys.* **2000**, *112*, 5292−5297.
(44) Grimme, S.; Antony, J.; Ehrlich, S.; Krieg, H. *J. Chem. Phys.* **2010**, *132*, 154104.
(45) Dion, M.; Rydberg, H.; Schröder, E.; Langreth, D. C.; Lundqvist, B. I. *Phys. Rev. Lett.* **2004**, *92*, 246401.
(46) Lee, K.; Murray, E. D.; Kong, L.; Lundqvist, B. I.; Langreth, D. C. *Phys. Rev. B* **2010**, *82*, 081101(R).
(47) Zhao, Y.; Truhlar, D. G. *Acc. Chem. Rev.* **2008**, *41*, 157−167.
(48) von Lilienfeld, O. A.; Tavernelli, I.; Röthlisberger, U.; Sebastiani, D. *Phys. Rev. Lett.* **2004**, *93*, 153004.
(49) Sun, Y. Y.; Kim, Y.-H.; Lee, K.; Zhang, S. B. *J. Chem. Phys.* **2006**, *124*, 174104.
(50) Stone, A. *The Theory of Intermolecular Forces*; Oxford University Press: New York, 1997.
(51) Wu, Q.; Yang, W. *J. Chem. Phys.* **2002**, *116*, 515−524.
(52) Grimme, S. *J. Comput. Chem.* **2004**, *25*, 1463−1473.
(53) Note that E^{disp} is only a model-dependent quantity with no real physical meaning. Dispersion energy is simply added to the total KS-DFT energy.
(54) Grimme, S. *J. Comput. Chem.* **2006**, *27*, 1787−1799.
(55) Jurečka, P.; Černý, J.; Hobza, P.; Salahub, D. R. *J. Comput. Chem.* **2007**, *28*, 555−569.
(56) Becke, A. D. *J. Chem. Phys.* **1997**, *107*, 8554−8560.
(57) Delley, B. *J. Chem. Phys.* **2000**, *113*, 7756−7764.
(58) Becke, A. D. *Phys. Rev. A* **1988**, *38*, 3098−3100.
(59) Lee., C.; Yang, W.; Parr, R. G. *Phys. Rev. B* **1988**, *37*, 785−789.
(60) (a) Perdew, J. P.; Wang, Y. *Phys. Rev. B* **1986**, *33*, 8800−8802. (b) Perdew, J. P. *Electronic Structure of Solids*; Ziesche, P., Eschrig, H., Ed.; Berling Academic: 1991.
(61) (a) Perdew, J. P.; Burke, K.; Ernzerhof, M. *Phys. Rev. Lett.* **1996**, *77*, 3865. (b) Perdew, J. P.; Burke, K.; Ernzerhof, M. *Phys. Rev. Lett.* **1997**, *78*, 1396E.
(62) Delley, B. *J. Chem. Phys.* **1990**, *92*, 508−517.
(63) Delley, B. *Modern Density Functional Theory: A Tool for Chemistry; Theoretical and Computational Chemistry*; Seminario, J. M., Politzer, P., Eds.; Elsevier: Amsterdam, 1995; Vol. *2*.
(64) Contreras-Torres, F. F.; Jalbout, A. F.; Jiménez-Fabian, I.; Amelines, O. F.; Basiuk, V. A. *J. Phys. Chem. C* **2008**, *112*, 2736−2742.
(65) Contreras-Torres, F. F.; Amelines-Sarria, O.; Jalbout, A. F.; Basiuk, E. V.; Basiuk, V. A. *Comput. Mater. Sci.* **2008**, *44*, 240−246.
(66) Contreras-Torres, F. F.; Basiuk, V. A.; Basiuk, E. V. *J. Comput. Theor. Nanosci.* **2010**, *7*, 408−413.
(67) Hariharan, P. C.; Pople, J. A. *Chem. Phys. Lett.* **1972**, *66*, 217−219.
(68) Frisch, M. J.; Trucks, G. W.; Schlegel, H. B.; Scuseria, G. E.; Robb, M. A.; Cheeseman, J. R.; Scalmani, G.; Barone, V.; Mennucci, B.; Petersson, G. A.; Nakatsuji, H.; Caricato, M.; Li, X.; Hratchian, H. P.; Izmaylov, A. F.; Bloino, J.; Zheng, G.; Sonnenberg, J. L.; Hada, M.; Ehara, M.; Toyota, K.; Fukuda, R.; Hasegawa, J.; Ishida, M.; Nakajima, T.; Honda, Y.; Kitao, O.; Nakai, H.; Vreven, T.; Montgomery, Jr., J. A.; Peralta, J. E.; Ogliaro, F.; Bearpark, M.; Heyd, J. J.; Brothers, E.; Kudin, K. N.; Staroverov, V. N.; Kobayashi, R.; Normand, J.; Raghavachari, K.; Rendell, A.; Burant, J. C.; Iyengar, S. S.; Tomasi, J.; Cossi, M.; Rega, N.; Millam, N. J.; Klene, M.; Knox, J. E.; Cross, J. B.; Bakken, V.; Adamo, C.; Jaramillo, J.; Gomperts, R.; Stratmann, R. E.; Yazyev, O.; Austin, A. J.; Cammi, R.; Pomelli, C.; Ochterski, J. W.; Martin, R. L.; Morokuma, K.; Zakrzewski, V. G.; Voth, G. A.; Salvador, P.; Dannenberg, J. J.; Dapprich, S.; Daniels, A. D.; Farkas, O.; Foresman, J. B.; Ortiz, J. V.; Cioslowski, J.; Fox, D. J. *Gaussian 09*, revision A.02; Gaussian, Inc.: Wallingford, CT, 2009.
(69) Halgren, T. A.; Lipscomb, W. N. *Chem. Phys. Lett.* **1977**, *49*, 225−232.
(70) Because of the fact that LSTCG technique performs a single LST maximization followed by a full conjugate gradient minimization, the total energies calculated by LSTCQ are lower than the ones calculated by the LST method. We note that quadratic synchronous transit (QST) methods also were explored; however, such algorithm as implemented in DMol3 code was unable to solve the SCF convergences relative to transition states.
(71) Basiuk, E. V.; Monroy-Peláez, M.; Puente-Lee, I.; Basiuk, V. A. *Nano Lett.* **2004**, *4*, 863−866.
(72) Basiuk, E. V.; Solis-González, O. A.; Alvarez-Zauco, E.; Puente-Lee, I.; Basiuk, V. A. *J. Nanosci. Nanotechnol.* **2009**, *9*, 3313−3319.
(73) Wesolowski, T. A.; Parisel, O.; Ellinger, Y.; Weber, J. *J. Phys. Chem A* **1997**, *101*, 7818−7825.
(74) Zhang, Y.; Pan, W. *J. Chem. Phys.* **1997**, *107*, 7921−7925.
(75) Hobza, P.; Šponer, J. *Chem. Rev.* **1999**, *99*, 3247−3276.
(76) Contreras-Torres, F. F.; Jalbout, A. F.; Amelines, O.; Basiuk, V. A. *J. Comput. Theor. Nanosci.* **2008**, *5*, 1367−1371.
(77) Masel, R. I. *Principles of Adsorption and Reaction on Solid Surfaces*; Wiley: New York, 1996.
(78) Briggs, J. B.; Montgomery, M.; Silva, L. L.; Miller, G. P. *Org. Lett.* **2005**, *7*, 5553−5555.
(79) Jens, A.; Grimme, S. *Phys. Chem. Chem. Phys.* **2006**, *8*, 5287−5293.
(80) Zhang, G.; Musgrave, C. B. *J. Phys. Chem. A* **2007**, *111*, 1554−1561.
(81) Petersilka, M.; Gross, E. K. U. *Int. J. Quantum Chem.* **1996**, *30*, 1393−1401.